Transfer standard for the spectral density of relative intensity noise of optical fiber sources near 1550 nm

Gregory E. Obarski and Jolene D. Splett

National Institute of Standards and Technology, Boulder, Colorado 80303

Received May 29, 2000; revised manuscript received December 11, 2000

We have developed a transfer standard for the spectral density of relative intensity noise (RIN) of optical fiber sources near 1550 nm. Amplified spontaneous emission (ASE) from an erbium-doped fiber amplifier (EDFA), when it is optically filtered over a narrow band (<5 nm), yields a stable RIN spectrum that is practically constant to several tens of gigahertz. The RIN is calculated from the power spectral density as measured with a calibrated optical spectrum analyzer. For a typical device it is −110 dB/Hz, with uncertainty ≤0.12 dB/Hz. The invariance of the RIN under attenuation yields a considerable dynamic range with respect to rf noise levels. Results are compared with those from a second method that uses a distributed-feedback laser (DFB) that has a Poisson-limited RIN. Application of each method to the same RIN measurement system yields frequency-dependent calibration functions that, when they are averaged, differ by ≤0.2 dB. © 2001 Optical Society of America

OCIS codes: 120.4800, 270.2500, 060.2330, 060.2320.

1. INTRODUCTION

Increasing demand for greater bandwidth in optical fiber communications has brought to fruition laser transmitters and optical fiber amplifiers with low-magnitude relative intensity noise (RIN) and noise figures, respectively. The noise figure of an optical amplifier can depend on the signal input RIN.[1] One can use a RIN measurement system that employs a rf spectrum analyzer in combination with a low-RIN laser (RIN < −160 dB/Hz) to determine the spectral density of the noise figure of a fiber amplifier. Such electrical methods are important because contributions of multiple path interference, which are neglected when optical techniques are used, are included in the noise figure measurement.[1–5] RIN can limit system performance in optical communications systems.[6–9] One can also use it to determine the resonance frequency, the intrinsic bandwidth, and the damping factor of lasers.[10] The appearance of commercial distributed-feedback (DFB) lasers and diode-pumped Nd:YAG lasers that have RINs with values of <−170 dB/Hz requires sensitive, accurate measurement systems. Thus we developed a transfer standard for precise calibration of RIN measurement systems that employ rf spectrum analyzers. The standard is an erbium-doped fiber amplifier (EDFA) to whose output are coupled a linear polarizer and a narrowband filter. We characterize a typical device for wavelengths near 1550 nm and rf frequencies in the 0.1–1.1-GHz range. The spectral density of RIN, however, is practically constant from zero to many tens of gigahertz, rendering it suitable for calibrations at even greater bandwidths.

The amplitude noise of the standard is amplified spontaneous emission (ASE) in the EDFA. Such fluctuations obey Bose–Einstein statistics, which can be approximated by thermal or Gaussian light.[11] The invariance of the spectral density of the RIN of thermal light under attenuation yields high accuracy and a considerable dynamic range with respect to rf noise levels; it also allows for the use of optical fiber connectors. The RIN of a typical device is −110 dB/Hz, with an uncertainty of <0.15 dB/Hz. To confirm the properties of the standard, we developed a second calibration method based on a DFB laser that has Poisson-limited RIN (see Section 8 below). Application of each method to a RIN measurement system yields frequency-dependent calibration functions (denoted Kappas herein) that are nearly identical in shape and whose equivalence can be derived by application of the RIN equations for each method to calibration of the RIN system. The difference between the Kappas of the two methods, averaged over a 1-GHz bandwidth, falls into the 0.04–0.2-dB range. Statistical tests demonstrate that the variability in Kappa of the two methods is similar. Thus the RIN standard compares favorably with that of a second method, i.e., the use of a Poisson-limited laser.

We denote the two EDFAs and the three filters used in this study EDFA1 and EDFA2, and F1, F2, and F3, respectively. A standard formed by EDFA2, F3, and linear polarizer P is written as EDFA2 + F3, with the P omitted; the polarizer is assumed present unless otherwise specified.

2. DEFINITION AND MEASUREMENT OF RELATIVE INTENSITY NOISE

RIN[9,12–14] can be precisely calculated from the autocorrelation integral of optical power fluctuations divided by total power squared. These temporal fluctuations can also be expressed in terms of their frequency spectrum by means of the Fourier transform of the autocorrelation integral. An optical source of output power $P(t)$ and fluc-

0740-3224/2001/060750-12$15.00

tuation $\delta P(t)$ has a total RIN, RIN_T, given by the ratio of the mean square of the fluctuation to the square of the average power:

$$\mathrm{RIN}_T = \frac{\langle \delta P(t)^2 \rangle}{\langle P(t) \rangle^2}, \tag{1}$$

where the time average $\langle \delta P(t)^2 \rangle$ arises from the autocorrelation function $\langle \delta P(t) \delta P(t + \tau) \rangle$ evaluated at time $\tau = 0$. The total RIN can be represented in the frequency domain by definition of a RIN spectral density, to which we refer simply as the RIN. Then RIN_T is also the integral of the RIN, $R(\nu)$, over all frequencies:

$$\mathrm{RIN}_T = \int_0^\infty R(\nu) \mathrm{d}\nu, \tag{2}$$

where ν is the optical frequency (in hertz). The spectral density of the RIN, $R(\nu)$, is derived by application of the Wiener–Khintchine theorem to the autocorrelation function $\lambda(\tau)$. By equating the right-hand sides of Eqs. (1) and (2), one can show that $R(\nu)$ is

$$R(\nu) = 2 \int_{-\infty}^{\infty} \lambda(\tau) \exp(i 2\pi\nu\tau) \mathrm{d}\tau. \tag{3}$$

Thus we define the RIN of an optical source to be the RIN spectral density $R(\nu)$ and the integral of the RIN to be the total RIN.

For classical states of light, the spectral density of amplitude fluctuations has a minimum of the standard Poisson limit, to which may be added some excess noise. Thus the RIN spectral density also consists of Poisson RIN and excess RIN. Whereas the excess RIN propagates unchanged through the system, the Poisson RIN depends on system losses. Expressed in terms of RIN, the standard quantum limit is the Poisson RIN. The total RIN is the sum of the spectral integrals of excess RIN and Poisson RIN.[15] Thus it is unitless. To develop a RIN standard we characterize two different RIN sources. The first source (RIN standard) is ASE from an EDFA, which can be approximated by thermal light. The second source is a laser with Poisson-limited RIN.

For light that obeys a Poisson distribution, the variance in the photon number is proportional to the photon number. Thus the square of the optical power fluctuations is proportional to the optical power. When it is represented by a single-sided noise spectrum, the Poisson RIN at a single optical frequency ν' is $2h\nu'/P_0$, where h is Planck's constant, ν is photon frequency, and P_0 is optical power. In electrical units it is $2q/i$, where q is the electron charge, $i = \eta q P_0/h\nu$ is the photocurrent, and η is the photodetector quantum efficiency. Thus the Poisson RIN in a real detection circuit increases as $1/\eta$.

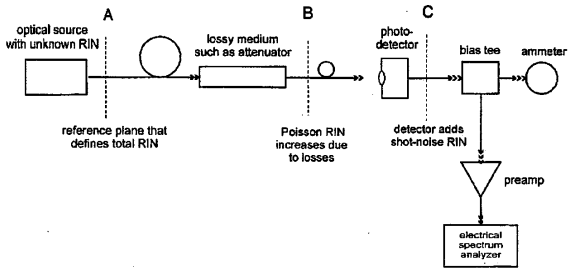

Fig. 1. Basic RIN measurement system.

A RIN measurement system is shown in Fig. 1. The beam traverses a lossy medium, such as an attenuator, and is collected by the photodetector. $R(\nu)$ is to be determined at reference plane A before any losses. The Poisson RIN increases at plane B as a result of losses and again at plane C because of inefficiency in the photodetection process. System efficiency can be combined into one factor, $\eta_T = \eta(1 - L)$, where L is the fractional loss before the detector. The excess RIN, however, propagates unchanged through the system. If $R_C(\nu)$ is the measured RIN at plane C, then the RIN is

$$R_A(\nu) = R_C(\nu) - (2q/i)(1 - \eta_T). \tag{4}$$

We determine the excess RIN, $R_{\mathrm{ex}}(\nu)$, by subtracting the measured Poisson or shot-noise RIN, $2q/i$, from $R_c(\nu)$, giving

$$R_{\mathrm{ex}}(\nu) = R_C(\nu) - 2q/i. \tag{5}$$

Equation (5) is equivalent to subtracting the Poisson RIN, represented here as $2h\nu'/P_0$, from the RIN at plane A:

$$R_{\mathrm{ex}}(\nu) = R_A(\nu) - 2h\nu'/P_0, \tag{6}$$

where P_0 is the laser power at plane A and ν' is the laser frequency.

Measuring RIN in the electrical domain entails using a bias tee to send the dc photocurrent to an ammeter while the ac noise is amplified and then displayed on a rf electrical spectrum analyzer (ESA). We denote the electrical frequency (referenced to the baseband) by f. Then the RIN is the noise power per unit bandwidth, $\delta P_e(f)$, weighted with the electrical frequency-dependent calibration function $\kappa(f)$ of the detection system and divided by the electrical dc power P_e. Thus

$$R(f) = \frac{\kappa(f) \delta P_e(f)}{P_e}, \tag{7}$$

where $\delta P_e(f)$ is the noise after subtraction of the thermal noise floor. Note that $\kappa(f)$ is proportional to the frequency response of the system and can be obtained by use of a broadband, flat source of known RIN.

3. FORM OF THE RELATIVE INTENSITY NOISE STANDARD AND A SECONDARY METHOD

The RIN transfer standard is shown in Fig. 2. The ASE from an EDFA is fed through a linear polarizer (P) followed by an optical filter (F) of 1–3-nm bandwidth, centered near 1550 nm.[16,17] The EDFA has a built-in optical isolator and was chosen for its semirugged qualities. To simplify operation for the customer, we arranged for a simplified front panel display with only an on–off power switch. The linear polarizer eliminates the potential for polarization imbalance between orthogonally polarized modes that might occur from fiber bending. The excess RIN of this device is much greater than the Poisson RIN, so the total RIN can be considered excess RIN. The shape and the bandwidth of the filter determine the RIN.

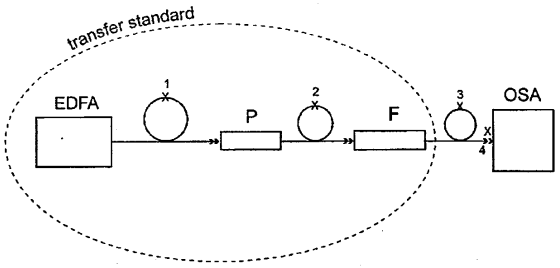

Fig. 2. Form of the RIN transfer standard; measurement of its OPSD with a calibrated OSA.

The optical power spectral density (OPSD) from the standard is measured by a diffraction-grating type of optical spectrum analyzer (OSA). For a single measurement, the OSA is set to average four sweeps on high sensitivity with the resolution bandwidth set at the minimum of 0.05 nm. High-quality threaded, physical-contact optical-fiber connectors and single-mode fiber are used. Points 1–4 represent locations where connectors were routinely disconnected to change components. Connector mating can change the power transmitted through the fiber link but not the RIN, which is invariant under attenuation.

4. PRINCIPLES

A. Spectral Density of the Relative Intensity Noise Standard

The spectral density of the RIN standard, as approximated by thermal or Gaussian light, must be obtained from a combination of measurement and theory-based calculation, as it cannot be measured directly. Although the spectral density theory has been developed,[11,18] we need an expression for the spectral density of RIN explicitly that correctly accounts for all scale factors.[19] We show that the RIN can be calculated from the OPSD as measured on an OSA. Contributions from the Poisson or standard quantum limit are considered negligible compared with those of the ASE.

It is well known that from the autocorrelation of the photocurrent fluctuations arises the frequency spectrum of the current fluctuations in terms of measurable quantities.[11,18] By application of the properties of the degree of coherence of the light field, the spectral density of the RIN can be expressed as an autocorrelation of a power spectral density function. For completeness we give the results for both polarized and unpolarized light, although we use the latter for the standard. For light that obeys Gaussian statistics, all space–time correlation functions of the field can be represented by ones of lower order.[11] An important result is that the second-order complex degree of coherence $\gamma(\tau)$, from which $\lambda(\tau)$ is derived, can be found from the first-order space–time correlation function. Thus the normalized intensity correlations for unpolarized thermal light at a single point in space can be derived from the degree of coherence:

$$\langle \Delta P(t)\Delta P(t+\tau)\rangle = (\langle P\rangle^2/2)|\gamma(\tau)|^2, \tag{8}$$

whereas for polarized thermal light

$$\langle \Delta P(t)\Delta(t+\tau)\rangle = \langle P\rangle^2|\gamma(\tau)|^2. \tag{9}$$

For unpolarized thermal light the autocorrelation of the intensity fluctuations in the time domain is

$$\lambda(\tau) \equiv \frac{\langle \Delta P(t)\Delta P(t+\tau)\rangle}{\langle P\rangle^2} = \frac{|\gamma(\tau)|^2}{2}. \tag{10}$$

Now the autocorrelation function of a stationary random process and the spectral density of the process form a Fourier-transform pair (Wiener–Khintchine theorem). Thus there exists a Fourier transform of $\gamma(\tau)$ in the frequency domain that is the normalized spectral density of the optical field[18]:

$$\phi(\nu) = \int_{-\infty}^{\infty} \gamma(\tau)\exp(-2\pi i\nu\tau)\mathrm{d}\tau. \tag{11}$$

Inasmuch as the Fourier transform in the frequency domain of the optical fields is zero for negative frequencies, one can show that $\phi(\nu)$ is single sided.[18] This is a natural result because $\phi(\nu)$ is the power spectrum or average energy density at a single point in space. Thus the inverse of $\phi(\nu)$ is

$$\gamma(\tau) = \int_0^{\infty} \phi(\nu)\exp(2\pi i\nu\tau)\mathrm{d}\nu. \tag{12}$$

From Eqs. (3) and (10), the RIN is

$$R(\nu) = \int_{-\infty}^{\infty} |\gamma(\tau)|^2\exp(2\pi i\nu\tau)\mathrm{d}\tau = \int_0^{\infty} \phi(\mu)\phi(\mu+\nu)\mathrm{d}\mu. \tag{13}$$

If $S(\nu)$ is the power spectral density as measured by the OSA, and P is the total power in the spectrum, then $\phi(\nu) = S(\nu)/P$, and the RIN for unpolarized thermal light is

$$R(f) = \int_0^{\infty} \frac{S(\nu)S(\nu+f)\mathrm{d}\nu}{P^2}. \tag{14}$$

For polarized thermal light we need only introduce the same factor of 2 that appears in Eq. (9) for the autocorrelation of the intensity fluctuations:

$$R(f) = 2\int_0^{\infty} \frac{S(\nu)S(\nu+f)\mathrm{d}\nu}{P^2}. \tag{15}$$

This result establishes the RIN standard of physical theory.

B. Numerical Expressions

We measured the power spectral density with a grating-type OSA that has a wavelength scale. However, we calculated the RIN in frequency units. Data points on the wavelength scale, λ, were converted to frequencies with $\lambda\nu = c$. Then each wavelength interval was converted to a frequency interval over the whole wavelength span. The RIN was calculated from Eq. (15).

We now develop a numerical expression for the RIN in the wavelength representation to illustrate the measurement process and because the uncertainty in the RIN was evaluated directly in wavelength units. If $\delta p_j(\lambda_j)$ is the

optical power measured at wavelength λ_j, where the resolution bandwidth is $B_j(\lambda_j)$, then the power spectral density $S_j(\lambda_j)$ at λ_j is

$$S_j(\lambda_j) = \frac{\delta P_j(\lambda_j)}{B_j(\lambda_j)}. \tag{16}$$

In the wavelength representation,

$$\mathrm{RIN}(\Lambda) \cong (2/P^2)\int_0^Z S(\lambda)S(\lambda + \Lambda)\mathrm{d}\lambda, \tag{17}$$

where P is the total optical power, λ is the wavelength, Z is the measurement span, and Λ is the shifting parameter in units of wavelength. The integral is not exact because λ and ν are inversely proportional. The resolution bandwidth, $B(\lambda)$, is converted to frequency units from the equation $\Delta\nu/\nu = -\Delta\lambda/\lambda$. Thus $B(\nu) = 1$ Hz corresponds to $B(\lambda) = \lambda^2/c$ in wavelength units, which can result in a considerable error in the RIN when the optical power is finite over ≈5 nm or more of the wavelength span.

Rewriting both the autocorrelation of the power spectral density and the optical power as sums, one can show that the RIN evaluated at some arbitrary wavelength shift Λ_i is

$$\mathrm{RIN}(\Lambda_i) = \frac{2\sum_j \frac{\delta P_j(\lambda_j)}{B_j(\lambda_j)}\frac{\delta P_{i+j}(\lambda_{i+j})}{B_{i+j}(\lambda_{i+j})}\Delta\lambda_j}{\left[\sum_j \frac{\delta P_j(\lambda_j)}{B_j(\lambda_j)}\Delta\lambda_j\right]^2}, \tag{18}$$

where $\Delta\lambda$ is the wavelength interval defined by division of the span by the number of data points minus 1. The shifting parameter does not appear explicitly but is defined to exist at the arbitrary shifting value of $\Lambda_i = \lambda_i$. Because the RIN of the standard is practically constant from zero shift to many tens of gigahertz, we can set $\Lambda_i = 0$, which implies that $i = 0$.

The total uncertainty in the RIN can be calculated from the appropriate versions of Eq. (18) as determined by the significant uncertainties in the parameters measured by the OSA. For example, the resolution bandwidth $B(\lambda)$ of our OSA turns out to be practically constant over the wavelength range of interest; thus it cancels in the RIN equation. If the wavelength distortion is also negligible, then $\Delta\lambda_j = \Delta\lambda$ and $B_j(\lambda_j) = B_{i+j}(\lambda_{i+j}) = B$ for all i and j. One can then show that at zero shifting the RIN reduces to

$$\mathrm{RIN} = \frac{2\sum_j \delta P_j(\lambda_j)^2}{\Delta\lambda\left[\sum_j \delta P_j(\lambda_j)\right]^2}. \tag{19}$$

5. PROPERTIES OF THE RELATIVE INTENSITY NOISE STANDARD

A. Polarization

When unpolarized thermal light is used, fiber bending can unbalance the power transmitted for orthogonally polarized modes and change the RIN by a finite amount. We attempted to measure this effect by changing the curvature of the fiber that links the various components but found the effect to be nearly negligible. Nonetheless, we add a polarizer to eliminate potential effects that might arise under various conditions. Furthermore, we have confirmed that the RIN for polarized thermal light increases by a factor of 2 compaired with that of unpolarized light. Measurement of the RIN with and without the linearly polarizing isolator gave a difference of 3.003 dB in noise power measured with an ESA. This result compares well with the 3.0103-dB difference predicted by theory. One need not calibrate the RIN system to perform this measurement because the calibration function cancels in the equations that define the difference in the RIN of the two states; it is necessary only that the measurement be performed at the same ESA settings.

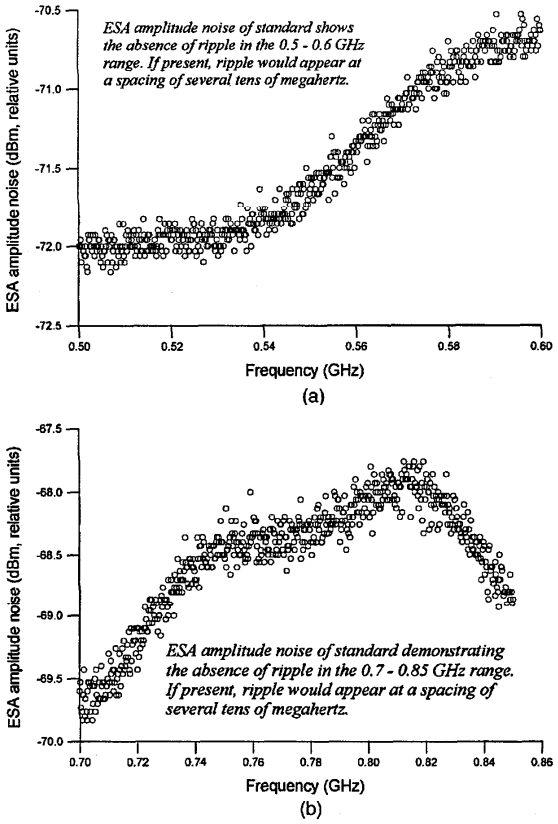

Fig. 3. Absence of ripple on the rf noise from the RIN standard over frequency bands (a) 0.5–0.6 GHz and (b) 0.7–0.85 GHz.

B. Absence of Ripple

A low-amplitude ripple of tens of megahertz was previously observed in EDFA's and attributed to multiple path interference.[20] To test for ripple we visually inspected the RIN spectrum with the ESA at several frequency spans. Figures 3(a) and 3(b) show the amplitude noise over the ranges of 0.5–0.6 GHz (data at intervals of ≈0.167 MHz) and 700–850 MHz (data at intervals of ≈0.25 MHz), respectively. Both figures are devoid of ripple. Sampling other frequency intervals, such as 500–600, 100–250, and 400–550 MHz (not shown), also

yielded no ripple. To further verify the absence of ripple, we note that a comparison of the calibration functions obtained from the standard and from the Poisson laser, an independent source without ripple (see Section 10 below), shows that the functions are nearly identical. Thus the built-in optical isolator effectively shields the EDFA from feedback.

C. Relative Intensity Noise of Various Filters of Different Transmittance Shapes

We solved the exact RIN spectral density equation for filters that had Gaussian, Lorentzian, and rectanglar shapes. For all three cases, $\mathrm{RIN}(f) = \mathrm{RIN}(0)$ up to a high frequency, and RIN(0) is inversely proportional to the bandwidth.[17] RIN calculations give similar results for filters of intermediate shape. However, the RIN of a filter with an asymmetric shape may behave differently.

Figure 4 shows the OPSD from EDFA2 with three different filters, F1–F3. Filter F1 is rectangular in shape and has a 3-dB bandwidth of 1.37 nm. Filter F2 is somewhat rectangular but spreads more quickly toward the wings; it has a bandwidth of 3.42 nm. Although filter F3 spreads quickly toward the wings, it has a 3-dB bandwidth of 1.32 nm. Figure 5 shows that the RIN obtained with all three filters is constant from zero to tens of gigahertz. The RIN from F1 falls off the fastest. Increasing the bandwidth (B) from 1.37 to 3.42 nm decreases the RIN. For F3, however, much of the power density exists far beyond the 3-dB points, so the contribution of the filter shape outweighs the $1/B$ dependence. The RIN of two additional filters (not shown) that have symmetrical shapes also followed a $1/B$ dependence. Figure 6 compares the RIN obtained from filter F1 connected to EDFA1 and to EDFA2. For both combinations the RIN is practically constant to several tens of gigahertz. The difference in RIN of −0.012 dB is very small, which may demonstrate that filter shape alone does not determine the RIN. The similar shape of the curves occurs because each curve arises from the same filter. The filter bandwidth is probably narrow enough to compensate for a potentially nonzero slope of the spectral density of a typical EDFA, which might occur over a wavelength interval of several nanometers about the center wavelength of the filter. If such an effect were significant, the RIN would not be constant.

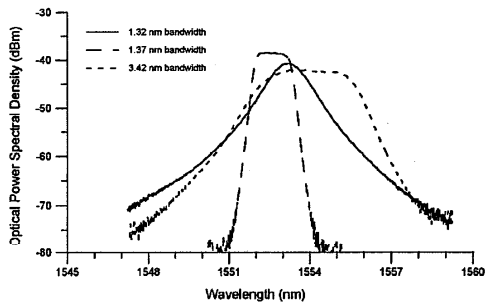

Fig. 4. OPSD of the three filters, F1 (1.37 nm), F2 (3.42 nm), and F3 (1.32 nm) used in this study.

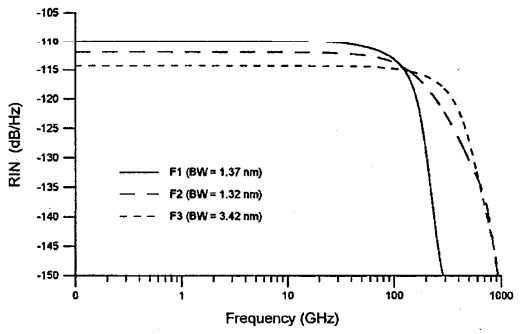

Fig. 5. RIN of F1–F3 from near zero to 1000 GHz with EDFA2.

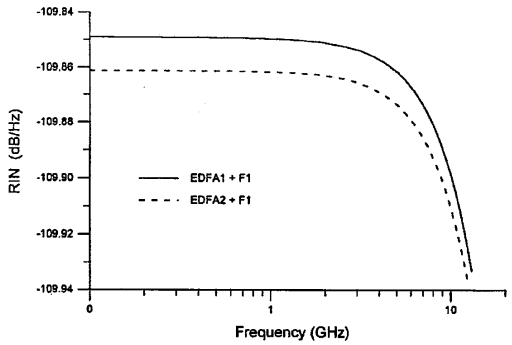

Fig. 6. Comparison of the RIN from F1 with EDFA1 and EFDA2.

D. Use of Fiber Connectors and Losses

The components that constitute a RIN standard can be joined by either fusion splicing or the more convenient but lossier fiber connectors. The effect of disconnecting and reconnecting components (on the RIN standard in aggregate) is a small change in the transmitted power spectral density. As the RIN is practically invariant under attenuation, we have chosen threaded, physical-contact optical fiber connectors.

6. CALIBRATION OF THE OPTICAL SPECTRUM ANALYZER

Equation (15) determines the RIN of the standard from the OPSD measured by the OSA (after the wavelength is converted to frequency units). The numerical equations for the RIN indicate that the OSA must be calibrated for resolution bandwidth, absolute wavelength and distortion, and spectral responsivity.

A. Resolution Bandwidth

We determined resolution bandwidth over a wide wavelength range by two distinct methods, using several narrow-linewidth lasers (linewidth, ≤instrument resolution bandwidth). Among these were a tunable laser (linewidth, <1 MHz) in the 1540–1580 nm range, with a wavelength measured by a high-accuracy wavemeter (1 part in 10^6), and a 1523-nm He–Ne laser (linewidth, <50 MHz; previously developed as a secondary wavelength standard). In one method, the response of the OSA to a narrow-linewidth laser (or to delta-function input) is read directly from the OSA. The single-wavelength input is

broadened by a monochrometer, and the resolution bandwidth is equated with the 3-dB bandwidth as read directly from the OSA. We refer to the broadened curve as the slit function. Figure 7 shows that the slit function for our OSA is fairly smooth from the peak value to ~25 dB below peak value, below which it becomes quite irregular. The 1-nm span is centered at 1551 nm, the resolution bandwidth is set at 0.05 nm, and the tunable laser is set at 3-mW optical power. In the second method, the noise equivalent bandwidth (denoted herein β) is calculated and used as the definition of resolution bandwidth. If λ_0 is the center wavelength of an arbitrarily shaped slit function $T(\lambda)$ of peak value $T(\lambda_0)$, then

$$\beta = \frac{1}{T(\lambda_0)} \int T(\lambda) d\lambda, \tag{20}$$

where integration is performed over the entire slit function with the background noise subtracted out. For a perfectly rectangular slit, either method gives the exact answer, whereas, for a distorted slit, β is more meaningful because it accounts for the same slit geometry.

For each method the tunable laser was set at a predetermined wavelength and the slit function displayed on the OSA. The two methods produce results that agree, as shown in Fig. 8. For either method, the resolution bandwidth is practically constant over the broad wavelength range. For the 3-dB method, the average resolution bandwidth (bw) is 0.041 nm, with a standard deviation (std dev) of 0.001 nm. For the noise equivalent bandwidth, the average is 0.045 nm, with the same standard deviation. We use the latter result because our slit function is irregular.

B. Wavelength Error and Distortion

The wavelength scale suffers distortion that manifests itself as a nonuniform distribution of wavelength points. We determined the absolute error and the distortion in the wavelength scale by comparing the wavelength from a narrow-linewidth tunable laser as read by the OSA with the known wavelength as read by a precision wavemeter. OSA data were averaged over four sweeps. For example, a wavelength setting of the tunable laser at 1560 nm yielded a value of 1559.975 nm when the wavelength was read by the wavemeter. The corresponding OSA wavelength reading was 1559.94 nm. The difference between the two results gives an uncertainty of 0.035 nm, which falls well within the manufacturer's specifications for wavelength, ±0.5 nm over the 350–1750-nm range. Wavelength error was measured for many points about both 1548 and 1560 nm. For the 21 points shown in Fig. 9, the standard deviation is 0.042 nm (in agreement with calibration results obtained by the manufacturer at specific wavelengths). For example, application of a He–Ne laser of 1523.1-nm wavelength (in air) yielded a wavelength reading of 1523.13 nm on the OSA. This is an error of 0.03 nm, in agreement with our average error of 0.042 nm.

C. Combined Effects of Attenuation, Pump Current, and Power Spectral Density Levels

Because the thermal RIN is a ratio of powers squared, and as such is invariant under attenuation, absolute power measurements are not required and thus calibration of the OSA is simplified, specifically for thermal RIN measurements. However, the potential effect on the RIN of a nonuniform power spectral density across the wavelength span of the OSA must be considered. In simplified numerical equation (19) for the RIN, a constant linear scaling error, say, ψ, would cancel if it were uniformly applied at every noise power, $\delta P_j(\lambda_j)$, over the entire wavelength span. In general, we expect ψ to arise mainly from the spectral responsivity of the OSA's photodetector combined with potential attenuation effects of wavelength dispersion from components or connectors in the fiber transmission line of the standard. As such, ψ is a measure of the total wavelength or frequency response of the OSA. On some level of fineness, we expect that $\psi_j = \psi_j(\lambda_j)$, so the uncertainty in noise power will not cancel. Thus we determined the uncertainty of spectral responsivity and attenuation in the aggregate and assigned the result as an upper bound for the spectral responsivity alone. In so doing, we determined the effect of ψ_j without measuring it explicitly.

The uncertainty that is due to noise power measurements was determined first by attenuation of the input RIN signal from the standard to fall at predetermined levels on the OSA screen. Attenuation of the RIN standard from 0 to 10 dB is shown in Fig. 10(a). The average RIN

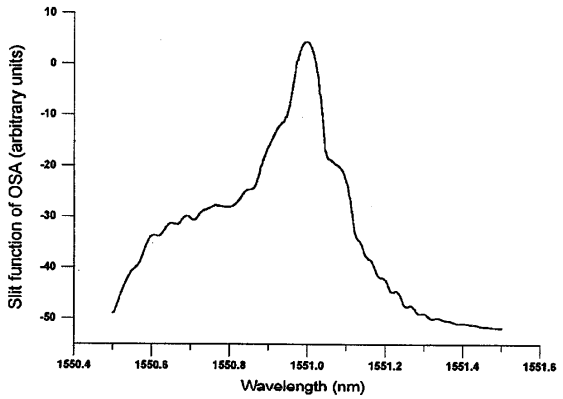

Fig. 7. Shape of the slit function of the OSA for a narrow-linewidth, tunable laser.

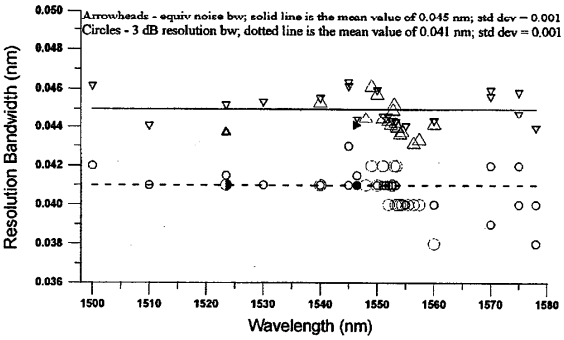

Fig. 8. Measurement of OSA resolution bandwidth versus wavelength as determined from the 3-dB bandwidth and the noise equivalent bandwidth for a narrow-linewidth, tunable laser.

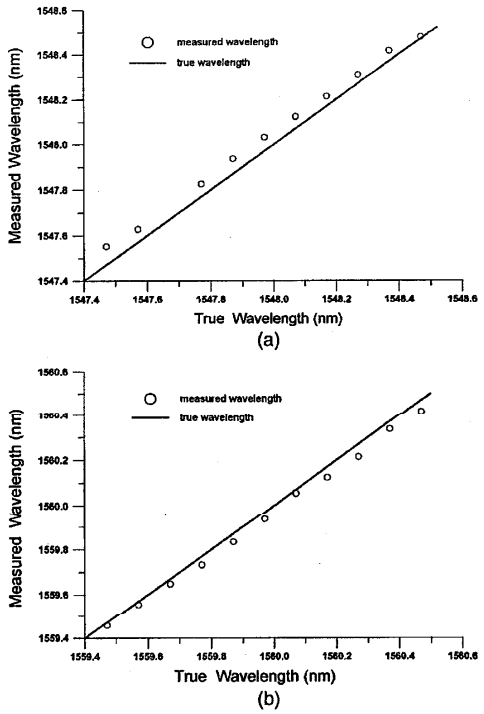

Fig. 9. Comparison of wavelengths measured by the OSA with the true wavelength in (a) the 1548-nm region and (b) the 1560-nm region.

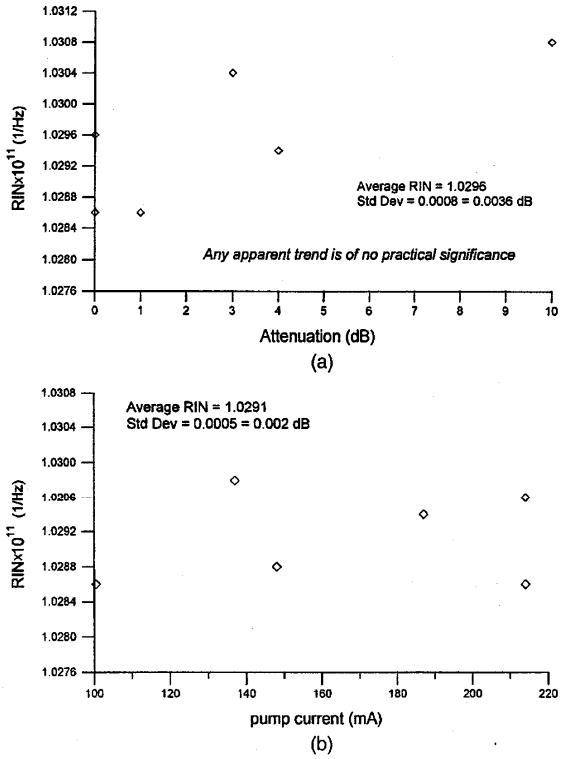

Fig. 10. RIN of EDFA1 + F1 versus (a) attenuation and (b) pump current.

Table 1. RIN for Various Values of Pump Current, Attenuation, and Intensity[a]

Pump Current (mA)	Attenuation (dB)	Intensity Relative To Maximum, I_{max} (dB)	RIN ($\times 10^{-12}\,Hz^{-1}$)
214	0	0	10.296
214	0	0	10.286
187	0	−1	10.294
148	0	−3	10.288
137	0	−4	10.298
100.5	0	−10	10.286
214	1	−1	10.286
214	3	−3	10.304
214	4	−4	10.294
214	10	−10	10.308
187	3	−4	10.308
149	1	−4	10.288
113	3	−10	10.298
185	10	−11	10.306
186	10	11	10.310

[a] To determine the effect of a nonlinear spectral responsivity, we adjusted some combinations of pump current and attenuation to give equal values of intensity on the OSA screen.

is $1.0296 \times 10^{-11}\,Hz^{-1}$ (−109.87 dB/Hz), with a standard deviation (Std Dev) of $0.0008 \times 10^{-11}\,Hz^{-1}$ (0.003 dB/Hz). To first order this result determines that the RIN is nearly invariant under practical attenuation strengths that may arise from component and connector losses. Figure 10(b) shows the variation in RIN with pump current at zero attenuation. The average RIN is $1.0291 \times 10^{-11}\,Hz^{-1}$ (109.87 dB/Hz), and the standard deviation is $0.0005 \times 10^{-11}\,Hz^{-1}$ (0.002 dB/Hz). Next we determined the RIN for a variety of pump currents, attenuation levels, and intensity levels, as listed in Table 1. For example, the effect of a variable attenuation could be studied with the spectral density held constant on the OSA screen by compensation of the pump current. For other measurements the intensity level was allowed to vary. Column 3 of Table 1 shows the intensity relative to the maximum, which occurs at zero attenuation and maximum pump current (214 mA). Thus the maximum intensity is represented by 0 dB, whereas 4 dB below the maximum appears as −4 dB. Such varied conditions again yielded nearly the same average value for the RIN, $1.0297 \times 10^{-11}\,Hz^{-1}$ (−109.87 dB/Hz), with a standard deviation of $0.002 \times 10^{-11}\,Hz^{-1}$ (0.008 dB/Hz), as when the intensity levels were allowed to vary on the screen. Thus the uncertainty in the RIN that is due to the uncertainties in spectral responsivity and attenuation in the aggregate is indeed very small.

7. UNCERTAINTY IN RIN OF THE TRANSFER STANDARD

The total uncertainty in the RIN standard is determined from the random error or repeatability of measurements[21]

and by the contributions of the OSA parameters to the OPSD measurement. The OSA's contribution is determined by application of the propagation of errors to the numerical RIN formulas of Section 6. The parameters that contribute significant errors are resolution bandwidth, wavelength distortion (absolute wavelength and wavelength interval), and spectral responsivity. Table 2 lists the various contributions to the total uncertainty. The quantities U_{REP}, U_{LIN}, U_{λ}, and U_{RBW} are the uncertainties that arise from the repeatability, linearity, wavelength distortion, and resolution bandwidth, respectively. The specific and combined standard uncertainties are shown in Table 2 for each filter. The RIN of the standard is the average of all RIN measurements used in computing U_{REP}. For filter F1 with 40 observations, $\langle RIN \rangle = 1.0325 \times 10^{-11}\,Hz^{-1}$. To compute the combined standard uncertainty of the average RIN, we add U_{REP}, U_{LIN}, U_{λ}, and U_{RBW} in quadrature. Because all four sources of uncertainty use measured data (as opposed to manufacturer's specifications, for example) to compute their values, they are all considered Type A uncertainties. Although different amplifiers were used to quantify U_{REP} and U_{LIN}, this should not influence the uncertainty estimates. The expanded uncertainty, U, is twice the combined standard uncertainty ($U = 2u_c$), which represents an approximate 95% confidence interval for the average RIN.[22] The combined standard uncertainty and expanded uncertainty for filters F1 and F2 are listed in Table 2. For F1 the combined standard uncertainty ($0.014475 \times 10^{-11}\,Hz^{-1}$) is 1.4% of the average RIN ($1.0325 \times 10^{-11}\,Hz^{-1}$). The average RIN for filter F2, $\langle RIN \rangle = 6.3712 \times 10^{-12}\,Hz^{-1}$, was based on 20 observations used to compute U_{REP}. The combined standard uncertainty ($0.053564 \times 10^{-12}\,Hz^{-1}$) is 0.84% of the average RIN.

8. POISSON-LIMITED LASER

Recall that any optical source can be rendered Poisson limited by sufficient attenuation[23] because the Poisson

Table 2. Combined Standard Uncertainty in the RIN of the Standard (EDFA2 with Filters F1 and F2)

Standard	Uncertainty Type (A or B)	Standard Uncertainty (×1/Hz)	Standard Uncertainty (dB)
EDFA2 + F1			
U_{REP}	A	0.000561×10^{-11}	0.002
U_{LIN}	A	0.001180×10^{-11}	0.005
U_{λ}	A	0.012315×10^{-11}	0.051
U_{RBW}	A	0.000419×10^{-11}	0.002
Combined, u_c	–	0.014475×10^{-11}	0.060
Expanded, U	–	0.029×10^{-11}	0.12
EDFA2 + F2			
U_{REP}	A	$0.0068325 \times 10^{-12}$	0.005
U_{LIN}	A	0.011804×10^{-12}	0.008
U_{λ}	A	0.025354×10^{-12}	0.017
U_{RBW}	A	0.009581×10^{-12}	0.006
Combined, u_c	–	0.053564×10^{-12}	0.036
Expanded, U	–	0.10713×10^{-12}	0.072

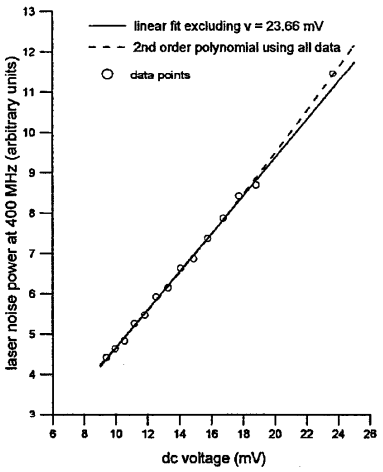

Fig. 11. Electrical noise power of a laser at 400 MHz versus dc voltage.

RIN increases with attenuation whereas the excess RIN remains invariant. Thus the Poisson limit is reached when the ratio of excess RIN to Poisson RIN vanishes. For an optical field at wavelength λ and power P_0 the Poisson RIN is

$$R_P(\omega) = R_p = \frac{2hc}{\lambda P_0} \approx \text{const.}, \tag{21}$$

where c is the speed of light and h is Planck's constant. A Poisson-limited source offers two distinct advantages over a low-excess-RIN source. First, the Poisson RIN manifests itself in the electrical detection circuit as the simple quantity $2q/i$. Second, a RIN system can be calibrated with a Poisson laser, without explicit knowledge of the RIN. Calibration of the RIN system yields a frequency-dependent calibration function that we have denoted Kappa (it is a dimensionless quantity, precisely defined in Section 9).

Application of relation (21) to a series of RIN measurements under attenuation demonstrates that the Poisson limit has been practically reached. Figure 11 shows the rf-noise power (in arbitrary units) at 400 MHz plotted versus dc voltage. Because Poisson-noise power is manifest in the electrical detection circuit as $2qv\Delta V = 2qV$ in a 1-Hz bandwidth (where V is voltage), the data should yield a straight line.[24] The voltage values range from 9.39 to 23.66 mV, with corresponding attenuations from 18 to 14 dB. The first curve is a second-order polynomial fitted to all data points. The second curve is a linear fit of all points except $V = 23.66$ mV (which corresponds to only 12-dB attenuation). The two curves rapidly converge to a straight line with increasing attenuation (decreasing voltage). At a voltage of 11.82 mV, where the attenuation is 17 dB, the curves are straight lines. This is the normal operating regime for this source. A second-order polynomial fit of all points except $V = 23.66$ mV yields a coefficient of nearly zero (slightly negative) for the second-order term. Thus the excess RIN component is too small to be resolved. (We note that the manufacturer specifies RIN ≤ -172 dB/Hz at the operating power of 27.82 mW. At 17-dB attenuation, accounting for all

losses, the Poisson RIN would be −149.2 dB/Hz and the excess RIN would remain ≤−172 dB/Hz. Thus the ratio of excess RIN to Poisson RIN would be ≤0.02 dB, well within the noise.)

9. CALIBRATION OF THE RELATIVE INTENSITY NOISE SYSTEM BY TWO DISTINCT METHODS

We developed two independent methods with which to calibrate a RIN measurement system, each using a precision RIN source. We can use a comparison of the results to evaluate the RIN standard. Because the distributions of photon number differ for the two methods, so too will the calibration functions. By formulating the RIN of each source both outside and inside the RIN system, we derive an exact equation that relates the system's response to the two independent sources. First we note a few simplifications. The amplitude fluctuations for the standard can be considered second-order only, that is, devoid of Poisson light. The laser RIN is practically Poisson limited, as was shown above.

A. Calibration Equations for the Standard and the Poisson Laser

We now derive the frequency-dependent calibration functions that govern the response of a RIN system to the input RIN of the standard and the Poisson laser, denoting them $\kappa_a(\omega)$ and $\kappa_p(\omega)$, respectively. Then we derive an equivalent Kappa that is common to both methods. Let δP_a and δP_p be the rf-noise powers measured by the ESA from the standard and the laser and P_a and P_p be the corresponding electrical dc powers. Let R_a be the RIN of the standard as calculated from the measured OPSD by the OSA and R_p be the RIN of the laser. Then, for the standard,

$$R_a(\omega) = R_a = \kappa_a(\omega)\frac{\delta P_a(\omega)}{P_a} \approx \text{const.} \tag{22}$$

Solving for κ_a gives

$$\kappa_a(\omega) = \frac{R_a P_a}{\delta P_a(\omega)}. \tag{23}$$

From expression (21), the Poisson RIN of the laser is $2hc/\lambda P_0$. Thus

$$R_p = \kappa_p(\omega)\frac{\delta P_p(\omega)}{P_p} = \frac{2hc}{\lambda P_0} \approx \text{const.}, \tag{24}$$

$$\kappa_p(\omega) = \frac{2hc}{\lambda P_0}\frac{P_p}{\delta P_p(\omega)}. \tag{25}$$

B. Equivalent Calibration Functions

To determine an equivalent Kappa that is common to both methods, recall that the Poisson RIN increases in the electrical detection circuit by an amount $1/\eta$. Therefore an equivalent optical RIN for the laser that would yield a Kappa that is equivalent to that for the standard, with all other conditions kept constant, is

$$\frac{R_p}{\eta} = \kappa_p(\omega)\frac{\delta P_p(\omega)}{P_p}, \tag{26}$$

where now $\kappa_a = \kappa_p$. Solving for κ_p gives

$$\kappa_p(\omega) = \frac{R_p P_p}{\eta \delta P_p(\omega)}. \tag{27}$$

Now the photocurrent in the electrical circuit is $i = \rho P_0 = \eta q P/h\nu$, where q is the electron charge and ρ and η are the responsivity and the quantum efficiency, respectively, of the photodetector. The dc voltage is $V = ir$, where r is resistance. When these expressions are substituted for current, and expression (24) for Poisson RIN, the quantum efficiency cancels, and we obtain

$$\kappa_p(\omega) = \frac{2qV}{\delta P_p(\omega)}. \tag{28}$$

Therefore

$$\kappa(\omega) = \frac{R_a P_a}{\delta P_a(\omega)} = \frac{2qV}{\delta P_p(\omega)}, \tag{29}$$

where we have now dropped the subscripts on Kappa. This analysis shows that κ_p can be determined without knowledge of the laser RIN or the quantum efficiency of the photodetector (measured at 0.77 at the operating wavelength of 1555.9 nm). For an actual calibration, the noise floor of the ESA is subtracted out.

10. COMPARISON OF THE STANDARD AND THE POISSON LASER

A. Agreement of Calibration Results

To evaluate the accuracy of the RIN standard we used it to calibrate our RIN measurement system and compared the results with those obtained with the laser. On a given day we determined Kappa for the standard and the laser as a pair of sequential measurement sets taken in the least time possible (which is ~2 min); this is the time needed to store the data for the standard, disconnect the standard, connect the laser, and collect the new data. This procedure ensures nearly identical environmental conditions (such as temperature and background rf fields) for the two methods. Stray rf signals can appear unpredictably in a data spectrum and arise from mobile tele-

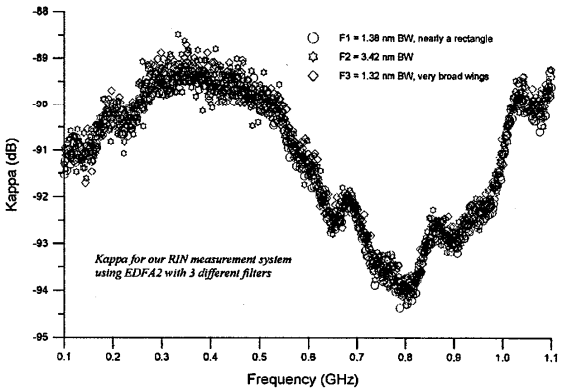

Fig. 12. Comparison of Kappas with EDFA2 and filters F1–F3.

phone sources, and the magnitude of the signals may vary during the time of a measurement. They must be averaged by manual inspection of the data. (The ESA data are averaged from nine sweeps, which takes ~20 s.) We used a variety of components to constitute a working standard. Among these were the six combinations that arise from the two EDFAs and the three filters discussed previously (Subsection 5.D). Figure 12 shows the results for Kappa obtained with EDFA2 with three filters of different shapes and bandwidths (1.32, 1.37, and 3.42 nm). The shape and overlap of the three sets of data confirms that our calculation of the RIN scales with filter bandwidth (BW) and shape, as expected from theory. The similarity of the three Kappas indicates that calibration of the RIN system is independent of the magnitude of the RIN and the shape of the filter. Next we compared the laser with F2 connected to EDFA1 or EDFA2. The results, shown in Fig. 13, are again similar.

To compare calibration methods quantitatively, we determined the simple average of the difference among Kappas recorded at all frequencies over the spectrum. Let $\kappa_{a,i}$ and $\kappa_{p,i}$ be the Kappas of the standard and of the laser at the ith frequency, f_i, respectively, and D_i the difference, $D_i - \kappa_{a,i} - \kappa_{p,i}$. If Z is the average difference obtained by summing over the 601 points in a spectrum, then

$$Z = \frac{\Sigma D_i}{601} = \frac{\Sigma(\kappa_{a,i} - \kappa_{p,i})}{601}. \tag{30}$$

Figure 14 shows a typical distribution of values of D obtained by comparison of EDFA1 + F2 with the laser. The differences range from −0.7 to 1 dB, with an average of 0.058 dB and a standard deviation of 0.3 dB. Table 3 compares calibration results obtained from various combinations of EDFAs and filters with one another and with

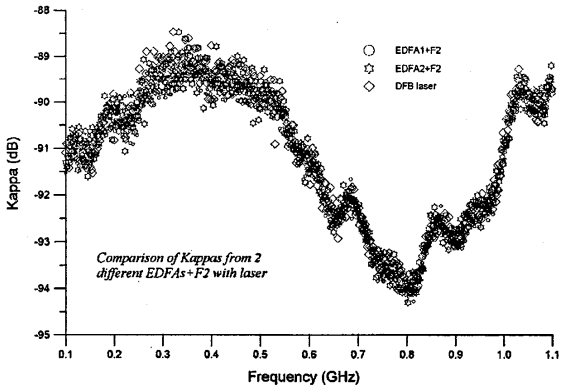

Fig. 13. Comparison of Kappas from the laser, EDFA1 + F2, and EDFA2 + F2.

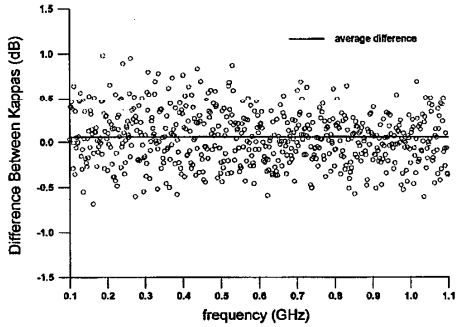

Fig. 14. Difference between Kappas from the laser and from EDFA1 + F2. The data range from −1 to +1 dB. The average difference is 0.058 dB.

Table 3. Comparison of Calibration Results Obtained with Various Combinations of EDFAs and Filters with One Another and with the Laser

Sources Compared	$Z = \frac{\Sigma D_i}{601} = \frac{\Sigma(\kappa_{a,i} - \kappa_{p,i})}{601}$	Standard Deviations of the Differences, D
Filters {F1 and F3}		
EDFA1 + F3 with EDFA2 + F3	−0.036	0.30
EDFA1 + F3 with DFB(3)	0.094	0.299
EDFA2 + F3 with DFB(3)	0.13	0.311
EDFA1 + F1 with EDFA2 + F1	0.041	0.198
EDFA1 + F1 with DFB(1)	0.113	0.248
EDFA2 + F1 with DFB(1)	0.071	0.249
EDFA1 + F1 with EDFA1 + F3	0.074	0.232
EDFA2 + F1 with EDFA2 + F3	0.025	0.252
DFB(1) and DFB(3)	0.0061	0.285
Filters {F2 and F3}		
EDFA1 + F2 with EDFA2 + F2	−0.074	0.349
EDFA1 + F2 with DFB(2)	0.058	0.302
EDFA2 + F2 with DFB(2)	0.143	0.35
EDFA1 + F3 with EDFA2 + F3	−0.056	0.295
EDFA1 + F3 with DFB(3)	0.076	0.271
EDFA2 + F3 with DFB(3)	0.131	0.301
EDFA1 + F2 with EDFA1+F3	0.105	0.268
EDFA2 + F2 with EDFA2 + F3	0.073	0.333
DFB(2) and DFB(3)	0.051	0.28

11. CONCLUSION

A transfer standard has been developed for the spectral density of the RIN of optical fiber sources in a 1550-nm range. The noise source is ASE from an EDFA that is coupled to a narrow-band optical filter and a linear polarizer. The RIN is obtained from a combination of measurement and theory, but it is also traceable to a second laboratory standard based on a laser's having Poisson-limited RIN. The standard is useful for accurate calibration of broadband RIN measurement systems.

APPENDIX A: CALIBRATION OF AN ELECTRICAL SPECTRUM ANALYZER

A RIN measurement system is calibrated with the transfer standard only, for a constant setting of the rf spectrum analyzer functions, such as sweep time, resolution and video bandwidth, and internal attenuation. Changing a function setting to accomodate a signal requires a new calibration because the Kappa obtained may differ slightly from the original. In addition, each ESA has a unique scale fidelity factor that accounts for the vertical position of the noise signal on the screen. RIN measurements for which the rf-amplitude noise differs must be weighted with this factor, which, like Kappa, is frequency dependent. The scale fidelity factor can be obtained by use of a rf signal generator, an attenuator, the ESA, and a rf power meter. Connector losses should be included and control settings kept the same as for a RIN measurement. The rf power is recorded at two positions on the ESA, with and without the attenuator. The scale fidelity correction for signals of various magnitudes can be expressed as a correction to Kappa at each frequency separately.[25]

ACKNOWLEDGMENTS

We are grateful to the following National Institute of Standards and Technology scientists: Wayne Itano for carefully verifying the mathematical expressions for the RIN of thermal light, Paul Hale for many stimulating discussions of various aspects of this research, and John Kitching, Richard Jones, and Jack Wang for valuable discussions. Jack Dupre of Agilent Technologies provided insight into calibration methods for optical spectrum analyzers.

G. E. Obarski's e-mail address is obarski@boulder.nist.gov.

REFERENCES AND NOTES

1. I. Jacobs, "Dependence of optical amplifier noise figure on relative-intensity-noise," J. Lightwave Technol. **13**, 1461–1465 (1995).
2. F. W. Willems and J. C. Van der Plaats, "Optical amplifier noise figure determination by signal RIN subtraction," in *Technical Digest–Symposium on Optical Fiber Measurements*, G. W. Day, D. L. Franzen, and R. K. Hickernall, eds., Natl. Inst. Stand. Technol. Spec. Publ. **864**, 7–9 (1994).
3. F. W. Willems and J. C. Van der Plaats, "Experimental demonstration of noise figure reduction caused by nonlinear photon statistics of saturated EDNAS," IEEE Photon. Technol. Lett. **7**, 488–490 (1995).
4. M. Movassaghi, M. K. Jackson, V. M. Smith, and W. J. Hallum, "Noise figure of erbium-doped fiber amplifiers in saturated operation," J. Lightwave Technol. **16**, 812–817 (1998).
5. M. Movassaghi, M. K. Jackson, V. M. Smith, J. F. Young, and W. J. Hallum, "Accurate frequency resolved measurement of EDFA noise figure," in *Optical Amplifiers and Their Applications*, A. Willner, M. Zervas, and S. Sasaki, eds., Vol. 16 of OSA Trends in Optics and Photonics Series (Optical Society of America, Washington D.C., 1997), pp. 130–133.
6. G. L. Koay, A. J. Lowery, R. S. Tucker, T. Higashi, S. Ogita, and H. Soda, "Data-rate dependence of suppression of reflection-induced intensity noise in Fabry–Perot semiconductor lasers," IEEE J. Quantum Electron. **31**, 1835–1839 (1995).
7. K. Y. Lau, C. M. Gee, T. R. Chen, N. Bar-Chaim, and I. Ury, "Signal-induced noise in fiber-optic links using directly modulated Fabry–Perot and distributed-feedback laser diodes," J. Lightwave Technol. **11**, 1216–1225 (1993).
8. I. Joindot, C. Boisrobert, and G. Kuhn, "Laser RIN calibration by extra noise injection," Electron. Lett. **25**, 1052–1053 (1989).
9. G. P. Agrawal, *Fiber-Optic Communications Systems* (Wiley, New York, 1992).
10. A. A. Saavedra, P.-J. Rigole, E. Goobar, R. Schatz, and S. Nilsson, "Relative intensity noise and linewidth measurements of a widely tunable GCSR laser," IEEE Photon. Technol. Lett. **10**, 481–483 (1998).
11. L. Mandel and E. Wolf, *Optical Coherence and Quantum Optics* (Cambridge U. Press, New York, 1995).
12. I. Joindot, "Measurement of relative intensity noise (RIN) in semiconductor lasers," J. Phys. III (Paris) **2**, 1591–1603 (1992).
13. I. Joindot, "Bruit relatif d'intensite des lasers a semiconducteur," Ph.D. dissertation (Universite des Sciences et Techniques du Languedoc, Languedoc, France 1990).
14. L. A. Coldren and S. W. Corzine, *Diode Lasers and Photonic Integrated Circuits* (Wiley, New York, 1995).
15. G. E. Obarski and P. D. Hale, "How to measure relative intensity noise in lasers," Laser Focus World, May 1999, pp. 273–277.
16. D. M. Baney, W. V. Sorin, and S. A. Newton, "High-frequency photodiode characterization using a filtered intensity noise technique," IEEE Photon. Technol. Lett. **6**, 1258–1260 (1994).
17. D. Baney and W. Sorin, "Broadband frequency characterization of optical receivers using intensity noise," Hewlett-Packard J., February 1995, pp. 6–12.
18. L. Mandel, "Fluctuations of light beams," in *Progress in Optics*, E. Wolf, ed. (North-Holland, Amsterdam, 1963), Vol. 2, pp. 181–248.
19. L. Mandel, Dept. of Physics and Astronomy, University of Rochester, Rochester, N.Y. 14627 (personal communications, June, 1999). Professor Mandel acknowledges an error of a factor of 2 in Eq. (9.8.26) of their text; see Ref. 11. The factor of 1/2 in front of the middle integral should be removed.
20. A. Girard, EXFO Fiber Optic Test Equipment Corporation, 465 Godin Avenue, Vanier, Quebec G1M 3G7 Canada (personal communications, January 1999).
21. "Analysis of variance," in *Guide to the Expression of Uncertainty in Measurement* (International Organization for Standardization, Geneva, Switzerland, 1993), Sec. H-5, pp. 85–87.
22. B. N. Taylor and C. E. Kuyatt, *Guidelines for Evaluating and Expressing the Uncertainty of NIST Measurement Results*, Natl. Inst. Stand. Technol. Tech. Note **1297** (1994).
23. S. Machida and Y. Yamamoto, "Quantum-limited operation of balanced mixer homodyne and heterodyne receivers," IEEE J. Quantum Electron. **QE-22**, 617–624 (1986).
24. M. C. Cox, N. J. Copener, and B. Williams, "High sensitivity precision relative intensity noise calibration standard using low noise reference laser source," IEE Proc. Sci. Meas. Technol. **145**, 163–165 (1998).
25. G. E. Obarski and J. D. Splett, "Measurement assurance program for the spectral density of relative intensity noise of optical fiber sources near 1550 nm," NIST Spec. Publ. 250–57 (2000).